Spin dynamics in the diluted ferromagnetic Kondo lattice model

Avinash Singh,[1,2,3,*] Subrat K. Das,[3] Anand Sharma,[1] and Wolfgang Nolting,[1]
[1]*Institut für Physik, Humboldt-Universität zu Berlin, Newton str. 15, D-12489 Berlin*
[2]*Max-Planck-Institut für Physik Komplexer Systeme, Nöthnitzer str. 38, D-01187 Dresden and*
[3]*Department of Physics, Indian Institute of Technology Kanpur - 208016*[*]

The interplay of disorder and competing interactions is investigated in the carrier-induced ferromagnetic state of the Kondo lattice model within a numerical finite-size study in which disorder is treated exactly. Competition between impurity spin couplings, stability of the ferromagnetic state, and magnetic transition temperature are quantitatively investigated in terms of magnon properties for different models including dilution, disorder, and weakly-coupled spins. A strong optimization is obtained for T_c at hole doping $p << x$, highlighting the importance of compensation in diluted magnetic semiconductors. The estimated T_c is in good agreement with experimental results for $\mathrm{Ga_{1-x}Mn_xAs}$ for corresponding impurity concentration, hole bandwidth, and compensation. Finite-temperature spin dynamics is quantitatively studied within a locally self-consistent magnon renormalization scheme, which yields a substantial enhancement in T_c due to spin clustering, and highlights the nearly-paramagnetic spin dynamics of weakly-coupled spins. The large enhancement in density of low-energy magnetic excitations due to disorder and competing interactions results in a strong thermal decay of magnetization, which fits well with the Bloch form $M_0(1-BT^{3/2})$ at low temperature, with B of same order of magnitude as obtained in recent squid magnetization measurements on $\mathrm{Ga_{1-x}Mn_xAs}$ samples.

I. INTRODUCTION

The discovery of ferromagnetism in diluted magnetic semiconductors (DMS) such as $\mathrm{Ga_{1-x}Mn_xAs}$,[1,2] with transition temperature $T_c \simeq 110$ K for Mn concentration $x \simeq 5\%$,[2,3] and $\simeq 150$ K in films for x in the range $6.7-8.5\%$,[4,5] has generated tremendous interest not only in view of potential technological applications, but also due to the novel ferromagnetism exhibited by these systems in which magnetic interaction between localized spins are mediated by doped carriers. The long-range oscillatory nature of the carrier-mediated spin couplings results in a variety of interesting behaviour such as significant sensitivity of spin stiffness and transition temperature T_c on carrier concentration, competing antiferromagnetic interaction and noncollinear ordering, spin-glass behaviour, spin clustering and disorder-induced localization etc.,[6–20] as recently reviewed.[21,22]

DMS such as $\mathrm{Ga_{1-x}Mn_xAs}$ are mixed spin-fermion systems in which the $S = 5/2$ $\mathrm{Mn^{++}}$ impurities replace $\mathrm{Ga^{+++}}$, thereby contributing a hole to the semiconductor valence band. However, large compensation due to As antisite defects reduces the hole density p to nearly 10% of Mn concentration x, which plays a key role in the stabilization of long-range ferromagnetic order, and also provides a complimentary limit to Kondo systems. The interplay between itinerant carriers in a partially filled band and the localized moments is conventionally studied within a diluted ferromagnetic Kondo lattice model (FKLM), wherein $-J\mathbf{S}_I.\boldsymbol{\sigma}_I$ represents the exchange interaction between the localized magnetic impurity spin $\mathbf{S}_I$ and the itinerant electron spin $\boldsymbol{\sigma}_I$.

Recently, finite-temperature spin dynamics due to thermal spin-wave excitations has been studied in $\mathrm{Ga}_{1-x}\mathrm{Mn}_x\mathrm{As}$ samples with different Mn content (thickness about 50nm, Mn content ranging from 2% to 6%) using SQUID (superconducting quantum interference device) magnetization measurements.[23] The temperature dependence of (low-field) spontaneous magnetization shows nearly linear fall off, similar to earlier results exhibiting even a distinct concave behaviour for unannealed samples,[3,4] possibly resulting from spin re-orientation transitions due to temperature-dependent magnetic anisotropies.[24] However, the spontaneous magnetization obtained using linear extrapolation from a 0.3-0.4 T magnetic field to overcome the anisotropy fields, discussed earlier for epitaxial ultra-thin Fe and FeCo films,[25] is found to be well described by the Bloch form $M(T) = M_0(1-BT^{3/2})$, with a spin-wave parameter $B \sim 1-3\times10^{-3}\ \mathrm{K}^{-2/3}$ which is about two orders of magnitude higher than for Fe and FeCo films. This large difference cannot be attributed only to a reduced exchange interaction. Post-growth annealing has been shown to significantly increase T_c, possibly due to enhancement of carrier concentration resulting from decrease of Mn interstitial concentration.[4] For a 50nm sample with 6% Mn, a decrease in B from $2.7\times10^{-3}\ \mathrm{K}^{-2/3}$ to $1.4\times10^{-3}\ \mathrm{K}^{-2/3}$ has also been obtained upon annealing,[23] with a corresponding increase in the spin-wave stiffness constant D from 53 meV$\AA^2$ to 71 meV$\AA^2$, which is of same order of magnitude as obtained from magnetic Kerr measurements using pump-probe setup of standing spin waves in ferromagnetic $\mathrm{Ga_{1-x}Mn_xAs}$ thin films.[26]

In view of these recent findings of strong thermal decay of magnetization in DMS systems, in this paper we investigate the interplay of disorder and competing interactions on magnon excitations in the diluted FKLM. We also study finite-temperature spin dynamics within a locally self-consistent magnon renormalization scheme, equivalent to a site-dependent Tyablikov decoupling (local RPA), and present the first site-dependent calculations for local impurity magnetization by explicitly incorporating the spatial feature of magnon states. As we shall see, the disorder-induced formation of low- and high-energy localized magnon modes, corresponding to weakly- and strongly-coupled spins respectively, results in a variety of interesting spin-dynamics behaviour, such as concave magnetization behaviour due to dominant nearly-paramagnetic contribution of weakly-coupled spins and an enhancement in T_c due to strong local correlations in impurity-spin clusters.

Within our non-perturbative approach, finite exchange interaction, impurity concentration, and disorder are treated on an equal footing. Impurity positional disorder is treated exactly by considering explicit realizations on finite-size systems and averaging over sufficiently large number of configurations to obtain statistically reliable results.

Magnon excitations provide a composite measure of the carrier-induced spin couplings in the collinear ferromagnetic state, with negative-energy modes signalling instability due to competing antiferromagnetic (AF) spin interactions. Magnon properties have been studied as function of electron density n in the conduction band and the spin-fermion coupling J within the concentrated FKLM (having a magnetic impurity at every lattice site) in the context of heavy fermion materials,[27] ferromagnetic metals Gd, Tb, Dy, doped EuX[28] and manganites.[29–32] In the context of DMS, magnon properties have been studied earlier in the random phase approximation (RPA) for the impurity-band model[10] and for the diluted Hubbard model[19,20] where disorder was treated exactly within finite-size numerical studies, and for the diluted FKLM within the virtual crystal approximation (VCA) where a uniform impurity-induced Zeeman splitting of the carrier spin bands is assumed,[9] within the coherent potential approximation (CPA),[12,33] and also for ordered impurity arrangements to make quantitative comparisons with different approximations.[34] Magnon spectrum and transition temperature have also been obtained recently for $\mathrm{Ga_{1-x}Mn_xAs}$ and $\mathrm{Ga_{1-x}Mn_xN}$ in terms of effective Heisenberg models with realistic exchange couplings, obtained recently from first-principle calculations as well.[35,36]

The organization of this paper is as follows. The RPA-level theory for magnon excitations in real space is derived in section II for a general fermion Hamiltonian, and the Goldstone-mode behaviour expected from spin-rotation symmetry is explicitly verified. Results for the diluted ferromagnetic Kondo lattice model are then discussed in Section III, with finite-temperature spin dynamics introduced in section IV. Conclusions are presented in section V.

II. MAGNON EXCITATIONS

Magnons represent transverse spin fluctuations about the spontaneously broken-symmetry state and constitute gapless, low-energy excitations for magnetic systems possessing continuous spin-rotational symmetry. At low temperature, magnons therefore play an important role in diverse macroscopic properties such as existence of long-range order, magnitude and temperature dependence of the order parameter, magnetic transition temperature, spin correlations etc. In the following we consider finite temperature T, and obtain magnon excitations at the RPA level where magnons interactions are neglected.

We consider the Kondo lattice model

$$H = H_0 - \frac{J}{2}\sum_I \mathbf{S}_I.\boldsymbol{\sigma}_I \tag{1}$$

where H_0 represents the free-fermion part consisting generally of hopping and on-site energy terms, and the second term represents the exchange coupling between impurity spins $\mathbf{S}_I$ and fermion spins $\boldsymbol{\sigma}_I/2$ at impurity sites I. The analysis presented below is independent of details of H_0, for which several cases of interest including dilution, hopping disorder, potential disorder, and multiple bands can be considered.

Applying the approximate Holstein-Primakoff transformation from the spin-lowering (S_I^-) and spin-raising (S_I^+) operators to boson (magnon) creation and annihilation operators $b_I^\dagger$ and b_I,

$$\begin{aligned} S_I^+ &= b_I\sqrt{2S_I} \\ S_I^- &= b_I^\dagger\sqrt{2S_I} \\ S_I^z &= S_I - b_I^\dagger b_I \end{aligned} \tag{2}$$

the Kondo lattice Hamiltonian reduces to

$$\begin{aligned} H &= H_0 \\ &-\frac{J}{2}\sum_I\left[\frac{\sqrt{2S_I}}{2}\left(b_I\sigma_I^- + b_I^\dagger\sigma_I^+\right) + \left(S_I - b_I^\dagger b_I\right)\sigma_I^z\right] \end{aligned} \tag{3}$$

where $\sigma_I^\pm \equiv \sigma_I^x \pm i\sigma_I^y$ and the "spin quantum numbers" $S_I \equiv \langle S_I^z\rangle_{\rm MF}$ refer to finite-temperature magnetizations obtained self consistently in the mean-field state. The above approximate transformation neglects quartic magnon interaction terms of order $1/S$.

Starting with a MF approximation, $\langle b_I^\dagger\rangle = \langle b_I\rangle = \langle b_I^\dagger b_I\rangle = 0$, the Hamiltonian (3) decouples into a fermion part with an impurity-field term

$$\mathcal{H}^0_{\rm fermion} = H_0 - \frac{J}{2}\sum_I S_I\sigma_I^z \tag{4}$$

and a local boson part

$$\mathcal{H}^0_{\rm boson} = \frac{J}{2}\sum_I \langle\sigma_I^z\rangle b_I^\dagger b_I \equiv \sum_I \mathcal{E}_I\, b_I^\dagger b_I\ , \tag{5}$$

representing the energy cost of a local spin deviation. At the MF level, determination of impurity and fermion magnetizations $\langle S_I^z\rangle$ and $\langle\sigma_I^z\rangle$ involves a self-consistent solution of the coupled spin-fermion problem in terms of

Brillouin and Fermi functions. In the zero-temperature limit, as $S_I \equiv \langle S_I^z \rangle_{\rm MF} = S$, the impurity magnetic field seen by fermions has same magnitude $JS/2$ on all sites, however, the magnetic field $J\langle \sigma_I^z \rangle_{\rm MF}/2$ seen by impurity spins remains non-uniform due to positional disorder.

Proceeding next to transverse spin fluctuations about the MF state, we obtain the time-ordered magnon propagator for the impurity spins in terms of the corresponding boson propagator

$$\begin{aligned}\mathcal{G}_{IJ}^{+-}(t-t') &= i\langle \Psi_{\rm G} \mid T[S_I^+(t)S_J^-(t')] \mid \Psi_{\rm G}\rangle \\ &= \sqrt{2S_I}\left(i\langle \Psi_{\rm G} \mid T[b_I(t)b_J^\dagger(t')] \mid \Psi_{\rm G}\rangle\right)\sqrt{2S_J} \qquad (6)\end{aligned}$$

at the RPA level by summing over all bubble diagrams

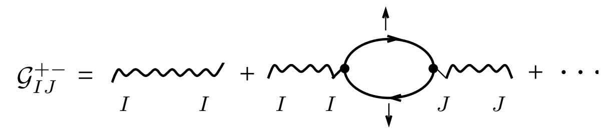

where the particle-hole bubble

$$\begin{aligned}[\chi^0(\omega)]_{IJ} &= i\int \frac{d\omega'}{2\pi}[G^\uparrow(\omega')]_{IJ}[G^\downarrow(\omega'-\omega)]_{JI} \\ &= \sum_{l,m} \frac{\psi_{l\uparrow}^I \psi_{l\uparrow}^J \psi_{m\downarrow}^I \psi_{m\downarrow}^J}{E_{m\downarrow} - E_{l\uparrow} + \omega}\, f_{l\uparrow}(1-f_{m\downarrow}) \\ &+ \sum_{l,m} \frac{\psi_{l\uparrow}^I \psi_{l\uparrow}^J \psi_{m\downarrow}^I \psi_{m\downarrow}^J}{E_{l\uparrow} - E_{m\downarrow} - \omega}\,(1-f_{l\uparrow})f_{m\downarrow} \qquad (7)\end{aligned}$$

with Fermi functions $f_{l\uparrow}$ and $f_{m\downarrow}$ involves integrating out the fermions (eigenvalues $\{E_{l\sigma}\}$ and wave functions $\{\psi_{l\sigma}\}$) in the broken-symmetry state. It is the particle-hole bubble $[\chi^0(\omega)]_{IJ}$ which mediates the carrier-induced impurity spin couplings in the ferromagnetic state, and the oscillatory, long-range nature of the spin couplings is effectively controlled by the fermion band filling and the impurity field strength.

In terms of the site-diagonal zeroth-order magnon propagator

$$[\mathcal{G}^0(\omega)] = \frac{[2S_I]}{\omega - \mathcal{H}^0_{\rm boson}} = \sum_I \frac{2S_I}{\omega - \mathcal{E}_I^0 + i\eta}|I\rangle\langle I| \qquad (8)$$

the full magnon propagator can then be expressed as

$$\begin{aligned}[\mathcal{G}^{+-}(\omega)] &= \frac{[\mathcal{G}^0(\omega)]}{1+\frac{J^2}{4}[\chi^0(\omega)][\mathcal{G}^0(\omega)]} \\ &= [\sqrt{2S_I}]\left(\frac{1}{\omega - [\mathcal{H}(\omega)]}\right)[\sqrt{2S_J}] \qquad (9)\end{aligned}$$

in terms of a boson "Hamiltonian"

$$[\mathcal{H}(\omega)]_{IJ} = \mathcal{E}_I\delta_{IJ} - \mathcal{E}_{IJ}(\omega) \qquad (10)$$

involving the boson on-site energy

$$\mathcal{E}_I \equiv \frac{J}{2}\langle \sigma_I^z \rangle \qquad (11)$$

and the boson hopping terms

$$\mathcal{E}_{IJ}(\omega) \equiv \sqrt{2S_I}\left(\frac{J^2}{4}[\chi^0(\omega)]_{IJ}\right)\sqrt{2S_J} \qquad (12)$$

associated with carrier-induced spin couplings $\mathcal{J}_{IJ} = (J^2/4)[\chi^0(\omega)]_{IJ}$. While dynamical effects are in principle included in the magnon Hamiltonian $[\mathcal{H}(\omega)]$, we find that the ω dependence is sufficiently weak to be neglected, so that the eigenvalues and eigenvectors of $[\mathcal{H}]$ directly yield the (bare) magnon energies $\{\omega_l^0\}$ and wave functions $\{\phi_l^0\}$.

Equation (9) has exactly same structure as obtained from the Tyablikov decoupling for an effective Heisenberg model with spin couplings $\mathcal{J}_{IJ} = (J^2/4)[\chi^0(\omega)]_{IJ}$, and readily yields a locally self-consistent renormalized magnon theory, as discussed in section IV.

In order to obtain a zero-energy Goldstone mode consistent with spin-rotation symmetry, the energy cost of creating a local spin deviation must be exactly offset by the delocalization-induced energy gain, and the corresponding condition

$$\frac{J}{2}\langle \sigma_I^z \rangle = \mathcal{E}_I = \sum_J \frac{J^2}{4}[\chi^0(\omega=0)]_{IJ}.2S_J \qquad (13)$$

is indeed exactly satisfied. This is easily verified in the concentrated limit where translational symmetry results in plane-wave fermion states with band energies $E_{\mathbf{k}\sigma} = \epsilon_{\mathbf{k}} - \sigma J\langle S^z\rangle/2$, and the particle-hole propagator (7) simplifies to

$$\begin{aligned}\chi^0(q,\omega=0) &= \sum_J [\chi^0(\omega=0)]_{IJ} \\ &= \sum_{\mathbf{k}} \frac{f_{\mathbf{k}\uparrow}(1-f_{\mathbf{k}\downarrow})}{J\langle S_z\rangle} + \frac{(1-f_{\mathbf{k}\uparrow})f_{\mathbf{k}\downarrow}}{-J\langle S_z\rangle} \\ &= \sum_{\mathbf{k}} \frac{(f_{\mathbf{k}\uparrow} - f_{\mathbf{k}\downarrow})}{J\langle S^z\rangle} = \frac{\langle \sigma^z\rangle}{J\langle S^z\rangle} \qquad (14)\end{aligned}$$

which ensures that the required condition (13) is satisfied. Quite generally, for a spin-rotationally-invariant system, condition (13) can be easily derived from a perturbative analysis for the transverse fermion-spin density induced by small transverse impurity fields (corresponding to small twist of the spin coordinate system), and then comparing with that expected on symmetry grounds.

The dimension of the magnon Hamiltonian $\mathcal{H}$ is N_m, the number of magnetic impurities per configuration. From the N_m magnon energies $\{\omega_l^0\}$ and wave functions $\{\phi_l^0\}$ we evaluate the magnon density of states and participtation ratio (PR)

$$\begin{aligned}N(\omega) &= \frac{1}{\pi}\frac{1}{N_m}\sum_l \frac{\eta}{(\omega-\omega_l^0)^2+\eta^2} \quad (\eta \to 0) \\ \text{PR} &= 1/\sum_I (\phi_l^{0I})^4 , \qquad (15)\end{aligned}$$

which together provide a complete picture of both spectral and spatial features of magnon states. The participation ratio provides a measure of the number of impurity spins over which the magnon state is extended. Generally, if the normalized wave function ϕ_l corresponds to a state with essentially non-zero amplitude $\phi_l^I \sim 1/\sqrt{n}$ on n sites, then PR$\sim n$. The participation ratio for magnon states can thus range between N_m for a fully extended magnon state and 1 for a site-localized magnon state. The PR thus readily allows localized magnon states (PR$\sim$ 1) to be distinguished from extended magnon states (PR$\sim N_m$).

We consider a simple cubic host lattice for simplicity, with periodic boundary conditions. We have considered system sizes $L = 8, 10, 12$, with the number of host lattice sites $N = L^3$ determining the dimension of the fermion Hamiltonian (4) to be diagonalized. Explicit realizations of random impurity arrangements are considered on the host lattice, for the given number N_m. In all cases we consider the saturated ferromagnetic state with a filled spin-$\uparrow$ band ($N_\uparrow = N$) and doping in the spin-$\downarrow$ band which is pushed up by the impurity Zeeman field. The impurity and carrier (hole) concentrations referred below correspond to $x = N_m/N$ and $p = (N - N_\downarrow)/N$, respectively.

III. DILUTED KONDO LATTICE MODEL

Providing a minimal description of the exchange coupling in DMS systems such as $Ga_{1-x}Mn_xAs$ between Mn impurity and carrier spins, the diluted ferromagnetic Kondo lattice model

$$H = t \sum_{i,\delta,\sigma} a_{i,\sigma}^\dagger a_{i+\delta,\sigma} + \epsilon_d \sum_{I,\sigma} a_{I,\sigma}^\dagger a_{I,\sigma} - \frac{J}{2} \sum_I \mathbf{S}_I . \boldsymbol{\sigma}_I \quad (16)$$

represents N_m magnetic impurities placed randomly on a fraction (I) of the N host sites (i). We consider a positive nearest-neighbour hopping t so that the host $\mathbf{k} = 0$ state lies at the top of the valence band; doped carriers (holes) go in long wavelength states, so that small-k particle-hole processes near the Fermi energy are dominant in the carrier-induced ferromagnetic spin couplings, and therefore other details of the energy band are relatively unimportant. In the following we set $t = 1$ as the unit of energy scale. Also, as the temperature regime of interest, set by the magnon energy scale, is very low compared to the MF energy scale, in the following we have only considered the $T = 0$ case which provides a good approximation of the low-temperature MF state.

Fermions see an effective potential disorder due to dilution; both disorder and dilution cannot be changed independently. We have therefore included an impurity on-site energy ϵ_d, which provides an effective control of disorder *independently* of dilution. For negative ϵ_d, the reduced impurity-site mean-field energy $(\epsilon_d + JS/2)$ for spin-$\downarrow$ fermions reduces the disparity between host and impurity sites, resulting in lower effective disorder (for $\epsilon_d = -JS/2$, there is no disorder at MF level!). The effects are quite dramatic on the magnon spectrum, showing significant decrease in the density of low-energy modes and hence enhanced stability of the carrier-mediated ferromagnetic state.

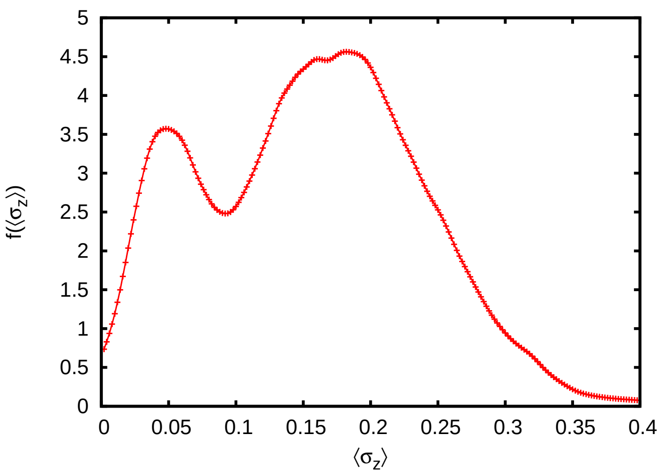

FIG. 1: Distribution of fermion spin densities on impurity sites, showing significantly reduced densities in impurity-poor regions relative to their average value $\approx p/x$. Here $J = 4$, hole doping $p \approx 4\%$ and impurity concentration $x \approx 20\%$.

The fermion spin polarization $\langle \sigma_I^z \rangle$ typically shows significant site variation as fermions tend to accumulate in impurity-rich regions. Figure 1 shows the distribution of fermion spin polarization on impurity sites, obtained by diagonalizing the fermion Hamiltonian (4) on a $N = 8^3$ system for 50 configurations. Besides the broad peak at the expected value of p/x corresponding to average hole density per impurity site, there is an additional peak at significantly reduced fermion spin polarization corresponding to impurity-poor regions; this introduces a new low-energy MF scale $J\langle \sigma_I^z \rangle S/2$ such that at comparable or higher temperatures these weakly-coupled impurity spins become nearly paramagnetic. However, as we shall see, the magnon energy scale is an order of magnitude smaller than even this low-energy MF scale, indicating that the dominant spin dynamics is due to thermal excitation of the collective magnetic excitations rather than that described by the Brillouin function corresponding to single-spin excitation energies within the MF theory. A self-consistent finite-temperature mean-field analysis is therefore not required, and the $T = 0$ description provides a good approximation of the low-temperature MF state.

Figure 2 shows the configuration-averaged magnon density of states (DOS) for two different hole doping concentrations and for varying degree of dilution. Initially dilution is seen to essentially broaden the magnon spectrum, but higher dilution results in significant softening of the collective excitations, with the magnon DOS peak progressively shifting to lower energy. Furthermore, this magnon softening is distinctly more pronounced at lower hole doping, reflecting more effective competition between longer-ranged spin couplings. In addition, new structure appears at higher energy, particularly at higher

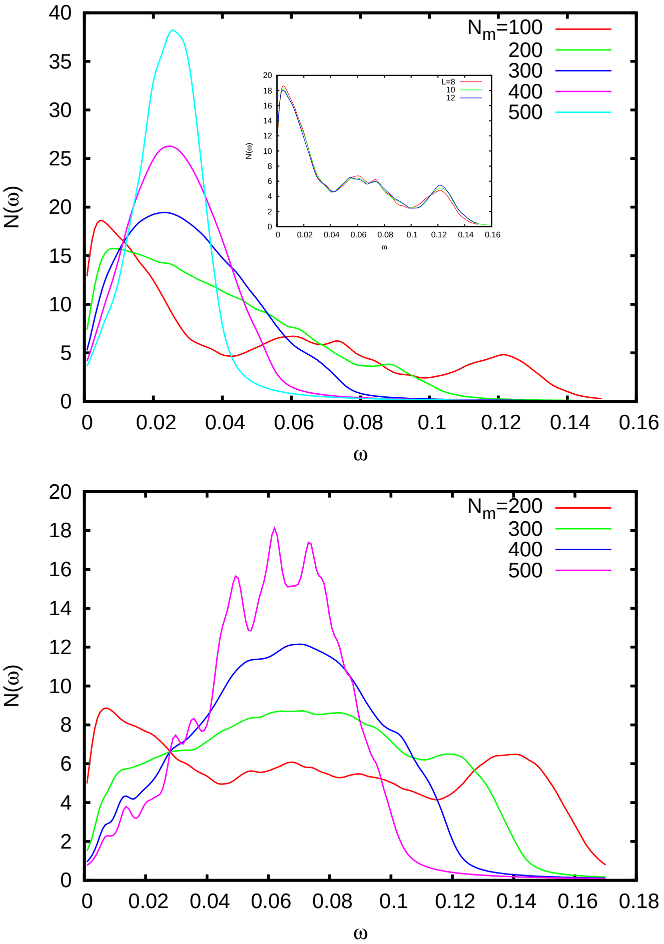

FIG. 2: Magnon density of states for different impurity dilutions for a $N = 8^3$ system with $J = 4$. The upper and lower panels correspond to hole doping $p \approx 4\%$ and $\approx 11\%$, respectively. Inset shows (for $x \approx 20\%$) comparison of magnon DOS for different system sizes $N = L^3$.

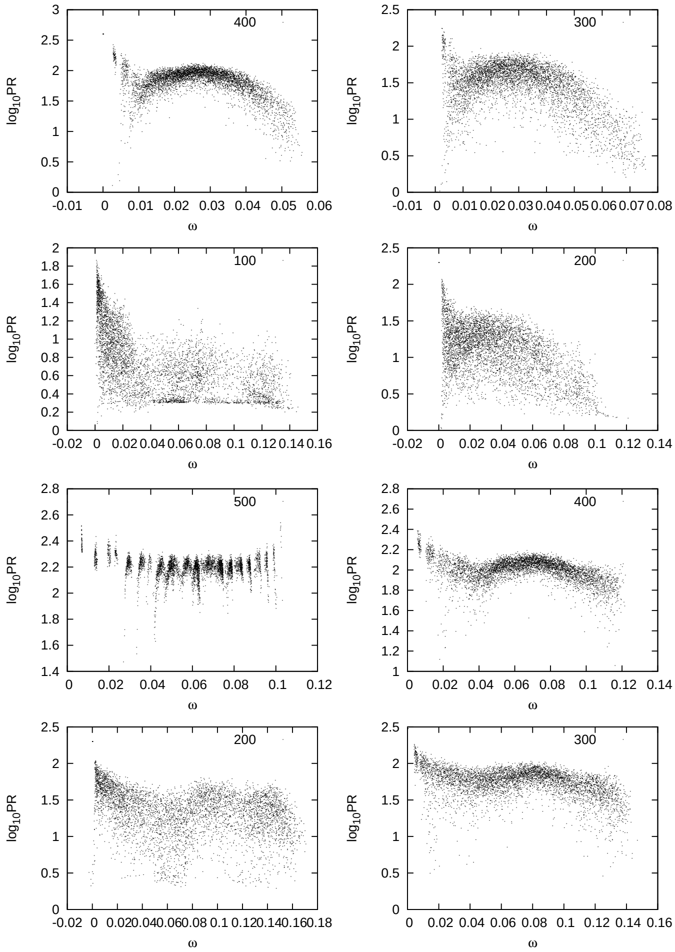

FIG. 3: Participation ratio for different impurity dilutions for a $N = 8^3$ system with $J = 4$ and hole concentrations $p \approx 4\%$ and $\approx 11\%$ in upper (four) and lower (four) panels, respectively.

dilution, which is due to localized magnon states associated with strongly-coupled spins in spin clusters, as also reported in earlier studies.[10,20] At still higher dilutions (not shown), negative-energy states appear in the magnon spectrum, indicating instability of the collinear ferromagnetic state. The correlation between spectral and spatial features of the magnon states is contained in the PR plots shown in Figure 3 for the two doping levels. In addition to the magnon softening with increasing dilution, the PR plots also show the increasing localization of magnon states with dilution, especially for the high-energy modes which are more likely to be localized over the strongly-coupled cluster spins.

We note here that the magnon energy scale for extended modes, which essentially determines the spin dynamics in the ordered state due to thermal excitations of magnons, is very low compared to the hopping energy scale, as low as around ~ 0.02 for the $x \approx 20\%$ case in Fig. 2. On the other hand, corresponding to reduced fermion polarization in impurity-poor regions, the low-energy MF scale is $J\langle\sigma_I^z\rangle S/2 \sim 0.25$. The nearly order-of-magnitude separation between these two energy scales implies, as discussed above, that the $T = 0$ calculations provide a good description of the low-temperature MF state.

Figure 4 shows effective control of impurity disorder at fixed dilution and doping. Enhanced potential disorder with increasing J results in magnon softening (upper panel), whereas negative ϵ_d effectively reduces disorder in the doped spin-$\downarrow$ band and results in magnon stiffening (lower panel), indicating stabilization of the ferromagnetic state and higher T_c.

Figure 5 shows the strong optimization of the transition temperature T_c with carrier concentration due to the characteristic competition between increasing overall magnitude of the carrier-induced spin couplings $J^2\chi^0_{IJ}$ and the increasing rapidity of its oscillation. Here we

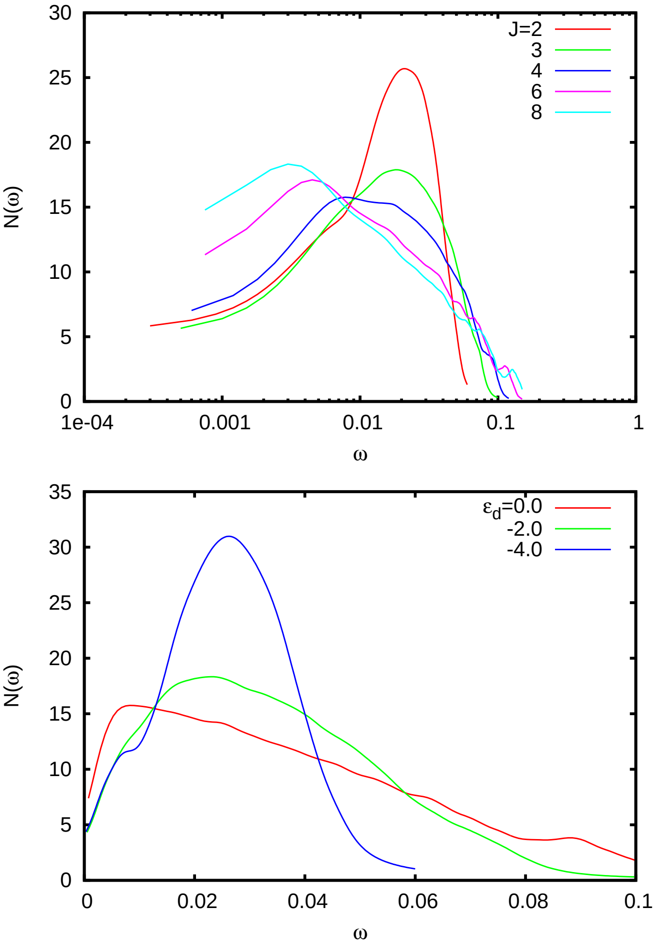

FIG. 4: Magnon density of states for different J and ϵ_d, showing effective control of impurity disorder independently of dilution, for a $N = 8^3$ system with $p \approx 4\%$, $x \approx 40\%$, and $\epsilon_d = 0$ and $J = 4.0$ in upper and lower panels, respectively.

have estimated T_c from the configuration average

$$\frac{1}{T_c} = \left\langle \frac{1}{N_m} \sum_l \frac{1}{\omega_l^0} \right\rangle_c \tag{17}$$

and taken a hole bandwidth ($W = 12t = 10$ eV) of the order of that of GaAs. Also, we have taken $x = 20\%$ for the impurity concentration (per unit cell for our sc lattice), corresponding to 5% Mn in the fcc system $Ga_{1-x}Mn_xAs$, which has 4 Ga sites per unit cell, and therefore impurity concentration $4x$ per unit cell. The peak at $p/x \sim 1/5$ shows the importance of compensation in DMS systems, and the calculated T_c is in good agreement with experimental results for $Ga_{1-x}Mn_xAs$.

The interplay of competing interactions and disorder is highlighted in Figure 6, which shows a comparison of magnon DOS and T_c for the ordered and disordered cases at the same dilution $x = 1/8$. Here the ordered case corresponds to a superlattice arrangement of impurities on alternate host lattice sites, studied earlier within a k-space sublattice-basis representation.[34] The low-energy

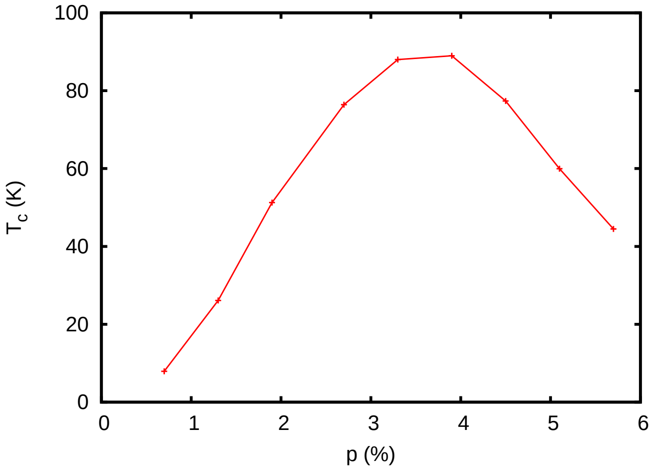

FIG. 5: Variation of T_c with hole concentration p for a $N = 10^3$ system with $J = 4$, $x = 20\%$, and carrier bandwidth $W = 12t = 10$ eV, averaged over 50 configurations.

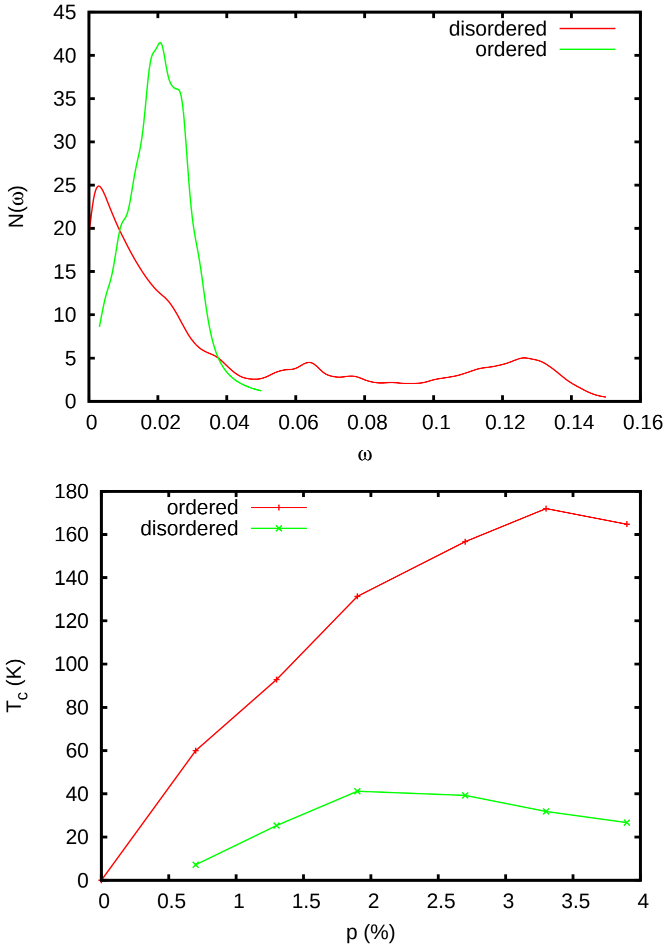

FIG. 6: Comparison of magnon DOS and T_c for the ordered and disordered cases with exactly same dilution $x = 1/8$, for a $N = 10^3$ system with $J = 4$. Here $p \approx 2.7\%$ in the upper panel and $W = 10$ eV in the lower panel.

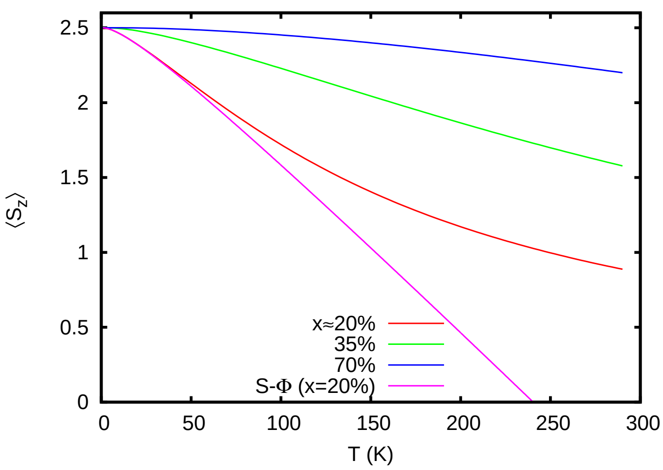

FIG. 7: Temperature dependence of averaged magnetization for different dilutions ($x \approx 20\%, 35\%, 70\%$) and system sizes ($N = 12^3, 10^3, 8^3$) while keeping the number of magnetic states fixed. Here $J = 4$, $W = 10$eV, and $p/x = 1/5$. Also shown is the conventional spin-wave-theory result (25).

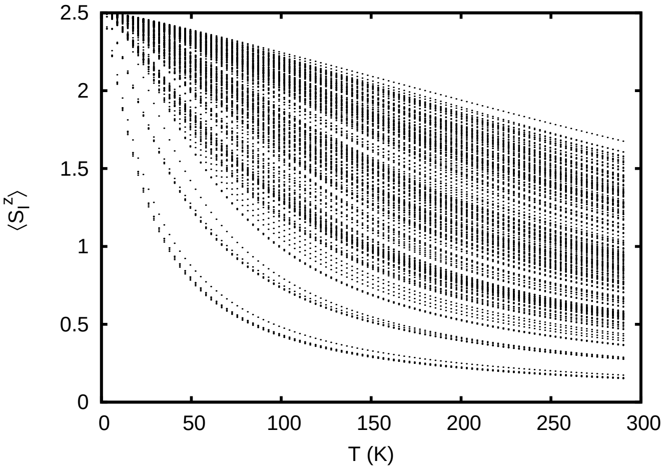

FIG. 8: Distribution of local magnetization, showing qualitatively different spin dynamics for weakly- and strongly-coupled spins in a $N = 10^3$ system with $J = 4$, $x = 20\%$, $p \approx 4\%$, and $W = 10$eV.

part of the magnon spectrum, which corresponds to extended modes, is seen to be significantly softened in the disordered case, resulting in substantially reduced T_c, and simply reflects the reduced spin stiffness due to competing interactions. The T_c result for the ordered case is in close agreement with earlier k-space analysis in terms of spin stiffness,[34] providing additional check on the validity of finite-size T_c calculations.

IV. FINITE-TEMPERATURE SPIN DYNAMICS

In section III we saw that dilution-induced disorder results in a strong enhancement in the density of low-energy magnons, with an appreciable fraction of localized modes corresponding to weakly-coupled spins, as well as formation of impurity-spin clusters supporting localized high-energy magnon modes. In order to quantitatively investigate the effect of these magnon features on the finite-temperature spin dynamics, in this section we evaluate the thermal reduction in magnetization due to magnon excitations.

We first discuss a locally self-consistent magnon renormalization scheme for the determination of local magnetizations, which is equivalent to the site-dependent Tyablikov decoupling procedure (local RPA) for a Heisenberg ferromagnet. We obtain the local magnetization from the Callen formula

$$\langle S_I^z \rangle = \frac{(S - \Phi_I)(1+\Phi_I)^{2S+1} + (S+1+\Phi_I)\Phi_I^{2S+1}}{(1+\Phi_I)^{2S+1} - \Phi_I^{2S+1}} \quad (18)$$

for a quantum spin-S ferromagnet,[38] where we have introduced site-dependent boson occupation numbers

$$\Phi_I = \frac{1}{N_m} \sum_l \frac{|\phi_l^I|^2}{e^{\beta\omega_l} - 1} \quad (19)$$

which explicitly involve the boson density $(\phi_l^I)^2$. A locally self-consistent magnon renormalization scheme (in terms of the fixed FKLM spin couplings $\mathcal{J}_{IJ} = (J^2/4)[\chi^0]_{IJ}$) is then obtained if the boson Hamiltonian matrix elements (10-13) are self-consistently renormalized

$$\begin{aligned} \mathcal{H}_{IJ} &= \sqrt{2\langle S_I^z \rangle} \left(\frac{J^2}{4}[\chi^0]_{IJ} \right) \sqrt{2\langle S_J^z \rangle} \\ \mathcal{H}_{II} &= \sum_{J \neq I} \left(\frac{J^2}{4}[\chi^0]_{IJ} \right) 2\langle S_J^z \rangle \end{aligned} \quad (20)$$

in terms of the local magnetization $\langle S_I^z \rangle$ instead of the MF values. Together with $\mathcal{H}|\phi_l\rangle = \omega_l|\phi_l\rangle$, the coupled equations (18-20) then self-consistently yield the local magnetization $\langle S_I^z \rangle$ for all sites. In the translationally-symmetric case this yields the usual momentum-independent magnon-energy renormalization $\omega_l = (\langle S^z \rangle / S)\omega_l^0$.

In the low-temperature regime, thermal magnon renormalization is negligible ($\langle S_I^z \rangle \to S$), and the bare ($T = 0$) magnon energies ω_l^0 provide a good description of the spin dynamics. We also have $\Phi_I << 1$, and the magnetization equation (18) reduces to the conventional spin-wave-theory result for the site-averaged magnetization

$$\langle S_z \rangle = S - \frac{1}{N_m} \sum_I \Phi_I = S - \int d\omega \frac{N(\omega)}{e^{\beta\omega} - 1}\,, \quad (21)$$

in terms of the bare magnon density of states $N(\omega)$. On the other hand, in an intermediate-temperature regime where $k_{\rm B}T \gg \omega_l^0$ for low-energy localized modes, then

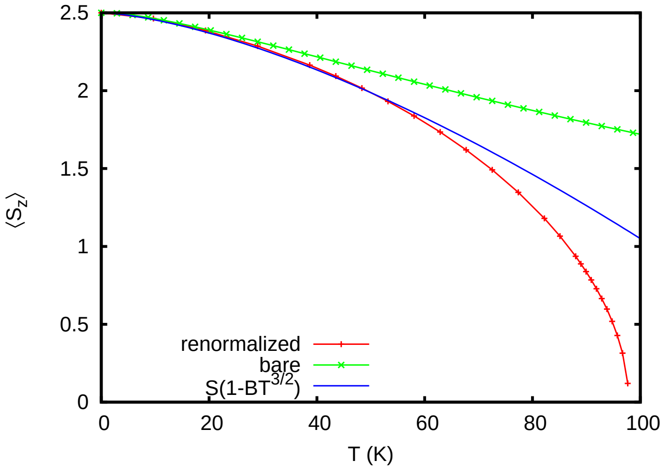

FIG. 9: Configuration-averaged magnetization within an approximate renormalization scheme involving the average boson occupation number, for a $N = 12^3$ system with $J = 4$, $W = 10$eV, $x \approx 20\%$, and $p \approx 4\%$, along with a fit with the Bloch form $S(1 - BT^{3/2})$, with $B = 0.6 \times 10^{-3}$ K$^{-2/3}$.

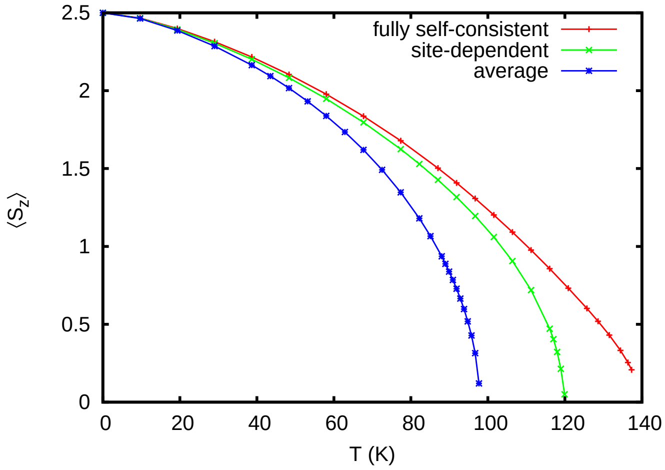

FIG. 10: Substantial enhancement in T_c due to spin clustering when the site-dependence of local magnon occupation number and magnetization is included, for a $N = 10^3$ system (single configuration), with $J = 4$, $W = 10$eV, $x = 20\%$, and $p \approx 4\%$.

$\Phi_I \sim k_{\rm B}T/\omega_l^0 >> 1$ and a nearly paramagnetic contribution $\langle S_I^z \rangle \sim \omega_l^0/k_{\rm B}T$ is obtained to the local magnetization, highlighting the qualitatively different spin dynamics of the isolated, weakly-coupled spins.

Figure 7 shows the temperature-dependence of magnetization evaluated from (18) and (19) with the bare ($T = 0$) magnon energies and wavefunctions and averaged over all impurity sites and several (20) configurations, for different dilutions ($x \approx 20\%, 35\%, 70\%$) and fixed value of $p/x = 1/5$. Different host system sizes $N = L^3$ with $L = 12, 10, 8$ are taken so that the number of magnetic states per configuration remains same ($N_m = 350$) in Eq. (19). The strong enhancement in the thermal decay of magnetization with dilution reflects the effect of the large enhancement in density of low-energy magnetic excitations on the finite-temperature spin dynamics. Also shown (for $x \approx 20\%$) is the conventional spin-wave-theory result (21), which asymptotically approaches the previous result in the low-temperature regime, as expected.

While the distinctly concave behaviour at higher temperature in the diluted case (Fig. 7, $x = 20\%$) is in itself not conclusive evidence for nearly paramagnetic behaviour of weakly-coupled spins, as similar behaviour would be obtained even for a translationally-symmetric system in a high-temperature ($k_{\rm B}T \gg \omega_l^0$) regime, the distribution of local magnetization $\langle S_I^z \rangle$ for a single configuration, clearly shows (Fig. 8) the qualitatively different spin dynamics for weakly- and strongly-coupled spins *for the same magnon spectrum*, thus highlighting the role of the spatial character of magnon states. The wide range of behaviour for different spins, and therefore the different local environments reflects the degree of complexity in a fully self-consistent magnon renormalization theory.

We next include magnon renormalization within an approximate scheme,[35] suitable for the low-temperature regime where $\langle S_I^z \rangle \sim S$ for all sites. Here the average magnetization $\langle S_z \rangle$ is self-consistently calculated from an equation similar to (18) in terms of the configuration- and site-averaged boson occupation number

$$\Phi \equiv \langle \Phi_I \rangle = \left\langle \frac{1}{N_m} \sum_l \frac{1}{e^{\beta(\langle S_z \rangle/S)\omega_l^0} - 1} \right\rangle_c \tag{22}$$

where the bare ($T = 0$) magnon energies ω_l^0 are uniformly renormalized by the factor $\langle S_z \rangle/S$, as in the standard Tyablikov theory. Figure 9 shows the temperature dependence of average magnetization obtained for several ($N_c = 20$) configurations of a $N = 12^3$ system with $J = 4$, $x \approx 20\%$, and $p \approx 4\%$. As expected, in the low-temperature regime where $\langle S_z \rangle \to S$ and $\Phi_I << 1$, the result approaches the previous (unrenormalized) result. Interestingly, the low-temperature behaviour of magnetization fits well with the Bloch form $S(1 - BT^{3/2})$, with $B = 0.6 \times 10^{-3}$ K$^{-2/3}$, which is of same order of magnitude (1.4×10^{-3} K$^{-2/3}$) as obtained in squid magnetization measurements of an annealed 50nm sample of $\rm Ga_{1-x}Mn_xAs$ with 6% Mn concentration.[23]

Dealing only with the average magnon occupation number, the above approximation does not incorporate the spatial segregation of magnon modes, particularly of the localization of high-energy modes over strongly-coupled cluster spins. Whereas, strong local correlations and high disordering temperature in these spin clusters should generally enhance long-range ordering and T_c, and therefore a quantitative analysis of this spin clustering is of interest. Localization of high-energy magnon modes over impurity clusters implies that cluster spins have relatively smaller participation in the low-energy modes, resulting in smaller magnon occupation number Φ_I and higher local magnetization $\langle S_I^z \rangle$ on cluster sites at low temperature. Fig. 10 shows the substantial enhancement in T_c resulting from including the site-dependence of Φ_I and $\langle S_I^z \rangle$, evaluated self-consistently from (18) and (19), but with a uniform magnon-energy renormalization $\omega_l = (\langle S^z \rangle / S)\omega_l^0$ in (19) in terms of the average magnetization $\langle S^z \rangle = (1/N_m)\sum_I \langle S_I^z \rangle$. Also shown is the result of the fully self-consistent magnon renormalization scheme (18-20), where the renormalized magnon energies ω_l and wave functions ϕ_l are obtained by diagonalizing the renormalized magnon Hamiltonian (20) which is updated at every step.

V. CONCLUSIONS

The exact treatment of disorder in our finite-size calculations allowed for a quantitative investigation of the interplay of disorder and competing interactions in the carrier-induced ferromagnetic state of the diluted ferromagnetic Kondo lattice model. Quantitative measures of the competition between impurity spin couplings, stability of the ferromagnetic state, and the magnetic transition temperature could be obtained from our real-space analysis of magnon excitations, with the estimated T_c in good agreement with experimental results for $\mathrm{Ga_{1-x}Mn_xAs}$ for corresponding impurity concentration, hole bandwidth, and compensation. Finite-temperature spin dynamics was studied within a locally self-consistent magnon renormalization scheme, equivalent to a site-dependent Tyablikov decoupling (local RPA), to investigate the role of magnon localization over isolated, weakly-coupled spins and over strongly-coupled cluster spins.

The strong magnon softening observed with dilution reflects increasingly effective competition between carrier-induced spin couplings, especially at lower hole doping where the couplings are longer-ranged. Indeed, the instability of the collinear ferromagnetic state at high dilution, as signalled by appearance of negative-energy magnon modes, indicates strong competition between ferromagnetic and antiferromagnetic spin couplings. Highlighting the importance of compensation in DMS systems, the strong optimization of T_c with hole doping at $p/x << 1$ stems from the competition between increasing overall magnitude and increasing rapidity of oscillation of the carrier-induced spin couplings. Comparison of the ordered and disordered cases for exactly same dilution, with significant magnon softening and lowering of T_c in the disordered case, explicitly demonstrates the interplay of disorder and competing interactions in DMS systems. The relatively milder magnon softening and robustness of ferromagnetic state obtained for purely potential disorder[39] serves to highlight the greater degree of frustration due to positional disorder in diluted systems.

The large enhancement in density of low-energy magnetic excitations arising from competing interactions and disorder is responsible for the strong thermal decay of magnetization at high dilution. While the distribution of local magnetization clearly exhibits spin-dynamics behaviour of both weakly- and strongly-coupled spins, the low-temperature behaviour of lattice-averaged magnetization was found to be dominated by low-energy extended magnon states, and fitted well with the Bloch form $M_0(1-BT^{3/2})$, with B of the same order of magnitude as obtained in recent squid magnetization measurements on $\mathrm{Ga_{1-x}Mn_xAs}$ samples.[23]

The enhancement in ferromagnetism due to strong local correlations in spin clusters is captured in the locally self-consistent magnon renormalization scheme, as reflected in the substantial enhancement in T_c obtained on including the site dependence of magnon occupation numbers. Furthermore, applied to the FKLM with a small fraction of weakly-coupled spins,[39] the scheme highlighted both the dominant nearly-paramagnetic spin dynamics of weakly-coupled spins in the low-temperature regime, and the dominant spin dynamics of bulk spins near T_c. Thus a wide range of spin-dynamics behaviour involving different local environments can be studied practically within the self-consistent magnon renormalization scheme.

Finally, we mention the outstanding and interesting issue of fermion-sector renormalization, in particular of the carrier-induced spin couplings due to quantum and thermal corrections to the bare particle-hole propagator $[\chi^0(\omega)]$. In the VCA-based approaches, the effective impurity field seen by fermions is taken to vanish as $T \to T_c$, yielding RKKY-type spin couplings. However, the large separation between moment-melting and moment-disordering temperatures implies presence of appreciable local moments even near T_c, so that fermions should continue to see impurity fields due to the slowly-fluctuating, locally-ordered impurity moments. Indeed, the splitting of fermion bands near T_c even for rather moderate couplings ($J/W \sim 0.2$), obtained within dynamical self-energy studies of the concentrated FKLM,[40] is precisely due to presence of the slowly-fluctuating impurity fields. It will be of interest to examine both quantum and thermal corrections to spin couplings due to self-energy and vertex corrections in $[\chi^0(\omega)]$ within a spin-rotationally invariant scheme which preserves the Goldstone mode. Studied recently for the ferromagnetic state of the Hubbard model,[37] the net quantum correction can be essentially understood in terms of an exchange-energy enhancement due to fermion spectral-weight transfer. Preliminary calculation of spectral-weight transfer for the FKLM indicates a suppresion by the factor $1/S$, suggesting relatively smaller quantum corrections for large spin quantum number S.

Acknowledgement

It is a pleasure to thank M. Sperl for communicating to us results prior to publication and G. X. Tang, J. Kienert, and S. Henning for helpful discussions. A. Singh acknowledges support from the Alexander von Humboldt Foundation.

* Electronic address: avinas@iitk.ac.in

[1] H. Ohno, A. Shen, F. Matsukara, A. Oiwa, A. Endo, S. Katsumoto, and Y. Iye, Appl. Phys. Lett. **69**, 363 (1996).
[2] F. Matsukara, H. Ohno, A. Shen, and Y. Sugawara, Phys. Rev. B **57**, R2037 (1998).
[3] H. Ohno and F. Matsukara, Solid State Commun. **117**, 179 (2003).
[4] K. C. Ku, S. J. Potashnik, R. F. Wang, S. H. Chun, P. Schiffer, N. Samarth, M. J. Seong, A. Mascarenhas, E. Johnston-Halperin, R. C. Myers, A. C. Gossard, and D. D. Awschalom, Appl. Phys. Lett. **82**, 2302 (2003).
[5] K. W. Edmonds, P. Boguslawski, K. Y. Wang, R. P. Campion, S. N. Novikov, N. R. S. Farley, B. L. Gallagher, C. T. Foxon, M. Sawicki, T. Dietl, M. B. Nardelli, and J. Bernholc, Phys. Rev. Lett. **92**, 037201 (2004).
[6] T. Dietl, A. Haury, and Y. M. d'Aubigne, Phys. Rev. B **55**, R3347 (1997); T. Dietl, H. Ohno, F. Matsukara, J. Cibert, and D. Ferrand, Science, **287**, 1019 (2000); T. Dietl, F. Matsukara, and H. Ohno, Phys. Rev. B **66**, 033203 (2002).
[7] M. Takahashi, Phys. Rev. B **56**, 7389 (1997).
[8] T. Jungworth, W. A. Atkinson, B. H. Lee, and A. H. MacDonald, Phys. Rev. B **59**, 9818 (1999); B. H. Lee, T. Jungworth, and A. H. MacDonald, *ibid* **61**, 15606 (2000).
[9] J. König, H. H. Lin, and A. H. MacDonald, Phys. Rev. Lett. **84**, 5628 (2000); J. König, T. Jungworth, and A. H. MacDonald, Phys. Rev. B **64**, 184423 (2001); J. Schliemann, J. König, and A. H. MacDonald, Phys. Rev. B **64**, 165201 (2001).
[10] M. Berciu and R. N. Bhatt, Phys. Rev. Lett. **87**, 107203 (2001); Phys. Rev. B **66**, 085207 (2002).
[11] A. Chattopadhyay, S. Das Sarma, and A. J. Millis, Phys. Rev. Lett. **87**, 227202 (2001).
[12] G. Bouzerar and T. P. Pareek, Phys. Rev. B **65**, 153203 (2002).
[13] J. Schliemann and A. H. MacDonald, Phys. Rev. Lett. **88**, 137201 (2002).
[14] A. L. Chudnovskiy and D. Pfannkuche, Phys. Rev. B **65**, 165216 (2002).
[15] C. Timm, F. Schäfer, and F. von Oppen, Phys. Rev. Lett. **89**, 137201 (2002); C. Timm and F. von Oppen, J. Supercond. **16** 23 (2003); cond-mat/0209055 (2002).
[16] M. P. Kennett, M. Berciu and R. N. Bhatt, Phys. Rev. B **65**, 115308 (2002); *ibid* **66**, 045207 (2002).
[17] G. Alvarez, M. Mayr, and E. Dagotto, Phys. Rev. Lett. **89**, 277202 (2002); G. Alvarez and E. Dagotto, Phys. Rev. B **68**, 045202 (2003).
[18] S. Das Sarma, E. H. Hwang, and A. Kaminski, Phys. Rev. B **67**, 155201 (2003); D. J. Priour, Jr., E. H. Hwang, and S. Das Sarma, Phys. Rev. Lett. **92**, 117201 (2004).
[19] A. Singh, A. Datta, S. K. Das, and V. A. Singh, Phys. Rev. B **68**, 235208 (2003).
[20] A. Singh, cond-mat/0307009 (2003).
[21] R. N. Bhatt, M. Berciu, M. P. Kennet, and X. Wan, Jour. of Superconductivity INM **15**, 71 (2002).
[22] C. Timm, J. Phys.: Condens. Matter **15**, R1865 (2003).
[23] M. Sperl, J. Sadowski, R. Gareev, W. Wegscheider, D. Weiss, and G. Bayreuther, to be published.
[24] M. Sawicki, K.-Y. Wang, K. W. Edmonds, R. P. Campion, C. R. Staddon, N. R. S. Farley, C. T. Foxon, E. Papis, E. Kamińska, A. Piotrowska, T. Dietl, and B. L. Gallagher, Phys. Rev. B **71**, 121302(R) (2005); M. Sawicki, J. Magn. Magn. Mater. **300**, 1 (2006).
[25] W. Kipferl, M. Sperl, T. Hagler, R. Meier, and G. Bayreuther, J. Appl. Phys. **97**, 10B313 (2005); M. Sperl, W. Kipferl, M. Dumm, and G. Bayreuther, *ibid* **99**, 08J703 (2006).
[26] D. M Wang, Y. H. Ren, R. Merlin, K. Dziatkowski, X. Liu, J. K. Furdyna, and M. Grimsditch, to appear in ICPS proceedings (2006).
[27] M. Sigrist and K. Ueda, and H. Tsunetsugu, Phys. Rev. B **46**, 175 (1992); M. Sigrist, H. Tsunetsugu, K. Ueda, and T. M. Rice, Phys. Rev. B **46**, 13838 (1992).
[28] M. Donath, P. A. Dowben, and W. Nolting, eds., *Magnetism and Electronic Correlations in Local-Moment Systems: Rare-Earth Elements and Compounds* (World Scientfic, Singapore, 1998).
[29] N. Furukawa, J. Phys. Soc. Jpn. **65**, 1174 (1996).
[30] X. Wang, Phys. Rev. B **57**, 7427 (1998).
[31] S. Yunoki, J. Hu, A. L. Malvezzi, A Moreo, N. Furukawa, and E. Dagotto, Phys. Rev. Lett. **80**, 845 (1998); E. Dagotto, S. Yunoki, A. L. Malvezzi, A. Moreo, J. Hu, S. Capponi, D. Poilblanc, and N. Furukawa, Phys. Rev. B **58**, 6414 (1998).
[32] M. Vogt, C. Santos, and W. Nolting, Phys. Stat. Sol. (b) **223**, 679 (2001).
[33] W. Nolting, T. Hickel, A. Ramakanth, G. G. Reddy, and M. Lipowczan, Phys. Rev. B **70**, 075207 (2004).
[34] S. K. Das and A. Singh, cond-mat/0506523 (2005).
[35] S. Hilbert and W. Nolting, Phys. Rev. B **70**, 165203 (2004); Phys. Rev. B **71**, 113204 (2005).
[36] G. Bouzerar, T. Ziman, and J. Kudrnovský, Europhys. Lett. **69**, 812 (2005); G. Bouzerar, T. Ziman, and J. Kudrnovský, Appl. Phys. Lett. **85**, 4941 (2004); R. Bouzerar, G. Bouzerar, and T. Ziman, Phys. Bev. B **73**, 024411 (2006).
[37] A. Singh, cond-mat/0512648.
[38] H. B. Callen, Phys. Rev. **130**, 890 (1963).
[39] A. Singh, S. K. Das, A. Sharma, and W. Nolting, cond-mat/0607633 (2006).
[40] W. Nolting, S. Rex, and S. Mathi Jaya, J. Phys. Cond. Matt. **9**, 1301 (1997).